Journal of Crystal Growth 456 (2016) 155–159

Contents lists available at ScienceDirect

Journal of Crystal Growth

journal homepage: www.elsevier.com/locate/jcrysgro

Preparation of high-quality AlN on sapphire by high-temperature face-to-face annealing

Hideto Miyake [a,b,*], Chia-Hung Lin [b], Kenta Tokoro [b], Kazumasa Hiramatsu [b]

[a] Graduate School of Regional Innovation Studies, Mie University, Mie 514-8507, Japan
[b] Department of Electrical and Electronic Engineering, Mie University, Mie 514-8507, Japan

ARTICLE INFO

Communicated by Jaime Andrade Freitas
Available online 10 August 2016

Keywords:
A1. Crystal morphology
A1. Recrystallization
A3. Physical vapor deposition processes
A3. Solid phase epitaxy
B1. Nitrides
B2. Semiconducting aluminum compounds

ABSTRACT

The annealing of sputtered AlN films with different thicknesses grown on sapphire in nitrogen ambient was investigated. In the annealing, two AlN films on sapphire were overlapped "face-to-face" to suppress the thermal decomposition of the AlN films. The sputtered AlN films with small grains consisted of columnar structure were initially aligned with (0002) orientation but became slightly inclined with increasing film thickness resulting in the formation of a two-layer structure. After annealing, films became a single crystalline layer regardless of the film thickness, and their crystallinity markedly improved after annealing at 1600–1700 °C. The full widths at half maximum of the (0002)- and ($10\bar{1}2$)-plane X-ray rocking curves were improved to 49 and 287 arcsec, respectively, owing to the annihilation of domain boundaries in the sputtered AlN films, which concurrently increased the compressive stress in the films.

1. Introduction

$Al_xGa_{1-x}N$ has great potential for use in optoelectronic devices in the deep-ultraviolet (DUV) region because of its wide direct band gap from 3.4 to 6.0 eV and excellent thermal and chemical stability [1–3]. However, $Al_xGa_{1-x}N$-based optoelectronic devices, such as light emitting diodes (LEDs) and laser diodes (LDs), have not been widely used owing to the absence of commercial substrates. High-crystal-quality AlN bulk substrates with an extremely low threading dislocation (TD) density ($<10^5\ cm^{-2}$) can be obtained by the sublimation–recondensation technique. Theses substrates are suitable for both LEDs and LDs [4–6]. Nevertheless, they still contain a high substitutional impurity concentration and have a higher cost and smaller size than AlN films grown on sapphire substrates. Meanwhile, AlN films grown on sapphire substrates suffer from a high density of TDs, which is mainly due to the large lattice and thermal coefficient mismatches between AlN and sapphire and also the different growth methods [the TD density in AlN films grown by metalorganic vapor epitaxy (MOVPE) is $>10^9\ cm^{-2}$], whereas that in the films grown by sputtering is $>10^{10}\ cm^{-2}$ [7,8]. Therefore, control of the growth of AlN its interface with the sapphire substrate is one of the key issues in obtaining high-efficiency UV optoelectronic devices [9,10].

Our group recently reported the formation of high-quality AlN films grown on sapphire substrates by MOVPE by thermal annealing at a high temperature in a carbon-saturated N_2-CO gas mixture [11]. The TD density in the AlN films was reduced to $4.7\times10^8\ cm^{-2}$, and the films can be used to fabricate conventional LEDs. However, there have been few reports on the high-temperature thermal annealing of sputtered AlN films grown on sapphire substrates, which has great potential for preparing highly uniform and large-scale AlN films for commercial use. In this work, we studied the effects of thermally annealing sputtered AlN films grown on sapphire substrates on the crystallinity and surface morphology, where the thermal annealing was performed in nitrogen ambient. The effects of annealing were investigated as a function of the sputtered AlN film thickness and the thermal annealing temperature.

2. Experimental

AlN films were grown on c-plane sapphire substrates by sputtering. The misorientation angle of the 2-inch substrates was $-0.2°$ toward the [$1\bar{1}00$] direction. AlN powder was used as a target, and the ambient was an argon (Ar) and nitrogen (N_2) gas mixture with the ratio [Ar]/[N_2]=0.33. The radio frequency (RF) power and growth temperature were 700 W and 650 °C, respectively. The thicknesses of the sputtered AlN films were 170 and 340 nm. Subsequently, the sputtered AlN films were thermally annealed in N_2 at 1600–1700 °C for 1 h. The surface of AlN film was covered with another sample as a setup of face-to-face or with a sapphire wafer to suppress the thermal decomposition of the AlN films, as shown in Fig. 1 [12]. The crystallinity of the AlN films and

* Corresponding author at: Graduate School of Regional Innovation Studies, Mie University, Mie 514-8507, Japan.

http://dx.doi.org/10.1016/j.jcrysgro.2016.08.028

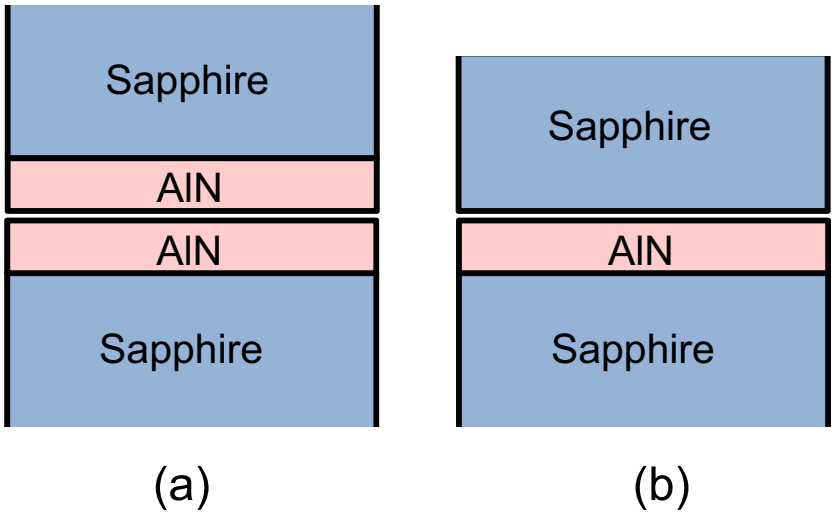

Fig. 1. Illustration of sample setup. (a) two AlN films on sapphire were overlapped "face-to-face", (b) The AlN film on sapphire was covered with sapphire wafer "AlN sandwich".

the lattice constants were determined by X-ray diffraction (XRD) analysis with an asymmetric Ge(220) monochromator for Cu K-alpha 1 (0.154 nm). The surface morphology and dislocation characterization were examined by atomic force microscopy (AFM) and transmission electron microscopy (TEM), respectively.

3. Results and discussion

Fig. 2 shows the (0002)- and (10$\bar{1}$2)-plane X-ray rocking curves (XRCs) for the sputtered AlN films with thicknesses of 170 and 340 nm. The integral intensities of both the (0002)- and (10$\bar{1}$2)-plane XRCs were higher for the thicker AlN films. The (0002)-plane XRC for the films with 170 nm thickness contains a higher-intensity sharp peak and a weak broad peak, whereas the intensity of the broad peak in the films with 340 nm thickness is higher, and the broad peak overlaps with the sharp peak. This result implies that the sputtered AlN films were aligned with (0002) orientation but became slightly inclined with increasing film thickness. This was probably due to the relaxation after the film reached a critical thickness of approximately 30–50 nm [13], and resulted in the formation of a two-layer structure as illustrated in Fig. 3. The growth mode of the sputtered AlN films is considered to be the Volmer–Weber (V–W) mode, which was determined by AFM measurement as shown in Fig. 4. Meanwhile, the (10$\bar{1}$2)-plane

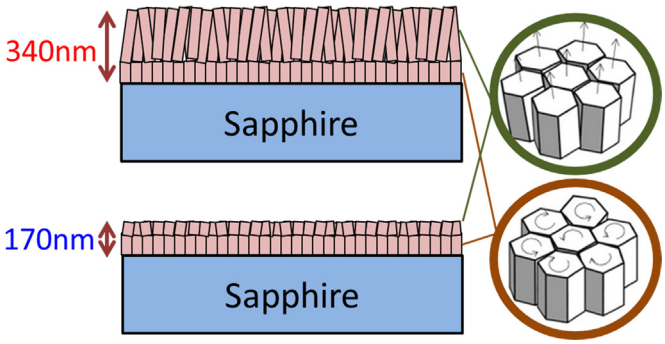

Fig. 3. Illustration of sputtered AlN films with thicknesses of 170 and 340 nm.

XRCs show only one broad peak for both the 170- and 340-nm-thick AlN films because of the high twist component in the sputtered AlN films in the case of low growth temperature during sputtering.

Fig. 4 shows AFM images of the 170- and 340-nm-thick sputtered AlN films without thermal annealing and with high-temperature thermal annealing at 1600–1700 °C. Tiny columnar-structure AlN films with a high density cover the entire surface before thermal annealing for both samples, demonstrating the highly uniform deposition of columnar-structure AlN films prepared by sputtering. These columnar-structure AlN films coalesced

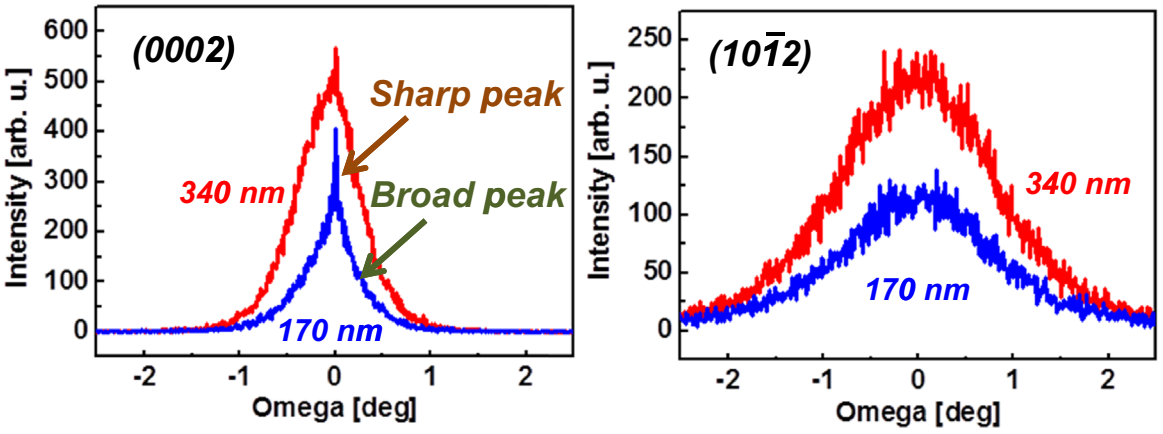

Fig. 2. The (0002)- and (10$\bar{1}$2)-plane XRCs for sputtered AlN films with thickness of 170 and 340 nm.

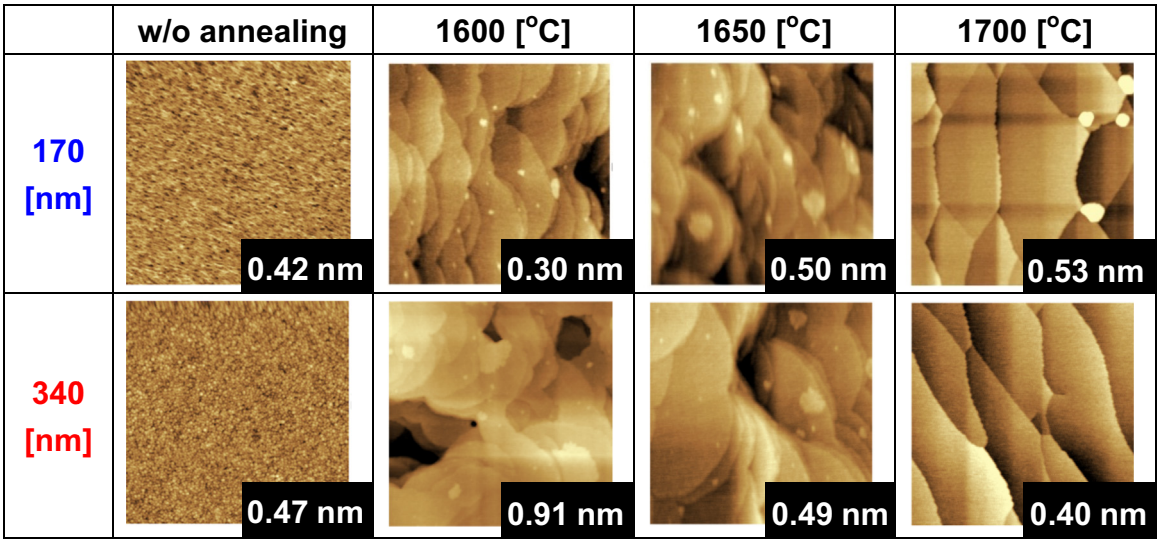

Fig. 4. AFM images of the 170- and 340-nm-thick sputtered AlN films without thermal annealing and with high-temperature thermal annealing at 1600 – 1700 °C. The scanning area used in the AFM was 1 μm×1 μm.

and formed a step and terrace surface morphology after thermal annealing at 1600 °C and above. No pits were observed on the terrace owing to the successful suppression of thermal decomposition of the AlN film by overlapping AlN samples face-to-face.

Fig. 5 shows the (0002)- and (10$\bar{1}$2)-plane XRCs for the 170-nm-thick sputtered AlN films without and with thermal annealing at 1700 °C. Both the (0002)- and (10$\bar{1}$2)-plane XRCs of the AlN films had a single sharp peak after thermal annealing owing to the elimination of the tilt and twist components from the sputtered AlN films by high-temperature thermal annealing. The improved crystallinity is related to the solid-phase reactions at that occur high annealing temperatures. The FWHMs of the (0002)- and (10$\bar{1}$2)-plane XRCs were markedly reduced from 532 to 49 and 6031 to 287 arcsec, respectively.

The FWHMs of the (0002)- and (10$\bar{1}$2)-plane XRCs for the AlN films with different thicknesses and thermal annealing temperatures are shown in Fig. 6. The FWHMs of the (0002)-plane XRCs for the AlN films with a thickness of 170 nm hardly changed with the annealing temperature whereas those for the AlN films with a thickness of 340 nm were similar at 1600 and 1650 °C but much lower at 1700 °C. This is due to the higher energy required for the alignment of thicker AlN films. On the other hand, the FWHMs of the (10$\bar{1}$2)-plane XRCs decreased with increasing annealing temperature for all samples. During the annealing, the columnar-structure AlN films coalesced, resulting in the annihilation of domain boundaries, thus improving the crystallinity of the AlN films. This result also corresponds to the transformation of the surface morphology from the columnar-structure AlN films to a step and terrace morphology by thermal annealing as shown in Fig. 4. The FWHMs of both the (0002)- and (10$\bar{1}$2)-plane XRCs eventually reach similar values for both the 170- and 340-nm-thick AlN films as the annealing temperature is increased to 1700 °C.

To further comprehend the mechanism of the coalescence of the columnar-structure AlN films during high-temperature thermal annealing, the *c*- and *a*-axis lattice constants are plotted for different thicknesses of the sputtered AlN film and thermal annealing temperatures in Fig. 7. The black square in the figure shows the lattice constant for an AlN bulk substrate for comparison (lattice constants for the AlN bulk: $a=3.112$ Å and $c=4.982$ Å). The *a*-axis lattice constant decreases and the *c*-axis lattice constant increases owing to the generation of compressive stress during thermal annealing. This stress increases with increasing thermal annealing temperature and decreasing film thickness because the former provides a higher energy and the latter lowers the barrier

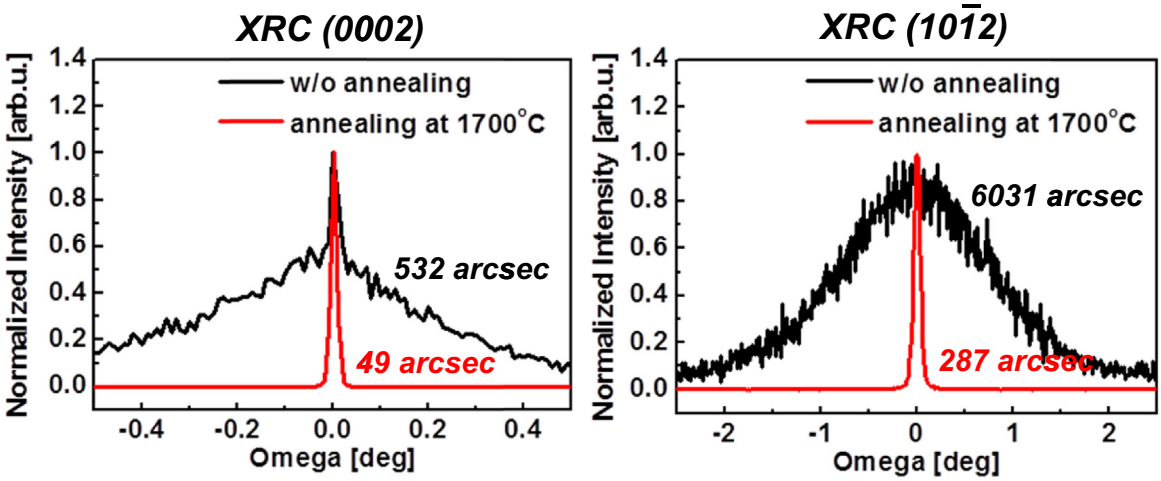

Fig. 5. The (0002)- and (10$\bar{1}$2)-plane XRCs for sputtered 170-nm-thick AlN films without and with thermal annealing at 1700 °C.

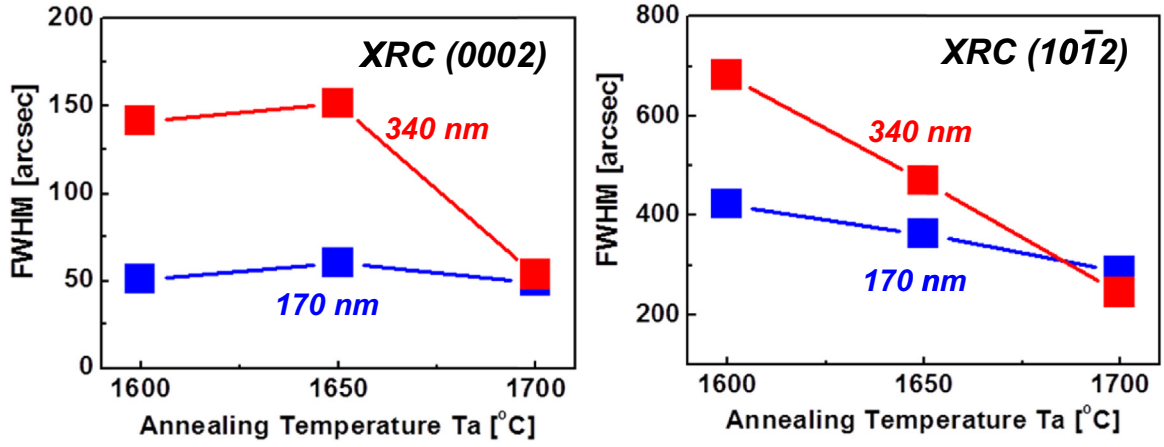

Fig. 6. FWHMs of (a) (0002)- and (b) (10$\bar{1}$2)-plane XRCs for the 170- and 340-nm-thick sputtered AlN films thermally annealed at 1600 – 1700 °C.

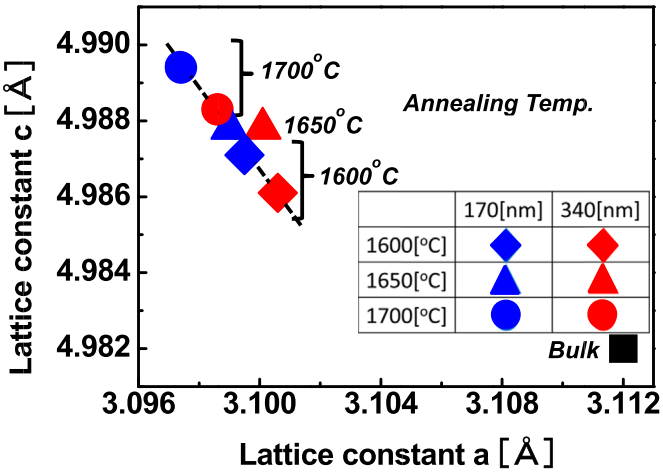

Fig. 7. *c*- and *a*-axis lattice constants plotted for different thicknesses of the sputtered AlN films and thermal annealing temperatures.

energy required for the coalescence of the sputtered columnar-structure AlN films.

Fig. 8 shows bright-field cross-sectional TEM images of the sputtered 340-nm-thick AlN films after thermal annealing at 1600 and 1700 °C. The types of TDs are characterized under the two-beam condition with $g=<0002>$ and $g=<1\,\bar{1}00>$. Type-***c*** (screw-type) and type-***a***+***c*** (mixed-type) dislocations are observable under $g=<0002>$, and type-***a*** (edge type) and type-***a***+***c*** dislocations are observable under $g=<1\bar{1}00>$ [14]. The TEM image of the sample annealed at 1600 °C obtained under the $g=<0002>$ indicates a higher TD density in the upper layer than that in the lower layer, which again indicates that the sputtering of AlN films generates a tilt component with increasing film thickness. The TEM images obtained under both the $g=<0002>$ and $g=<1\,\bar{1}00>$ indicates that the TD density decreases with increasing annealing temperature from 1600 to 1700 °C, which is also consistent with the FWHMs of the XRCs shown in Fig. 6. This result shows that the dislocations in the AlN buffer layer were indeed annihilated by thermal annealing at 1700 °C.

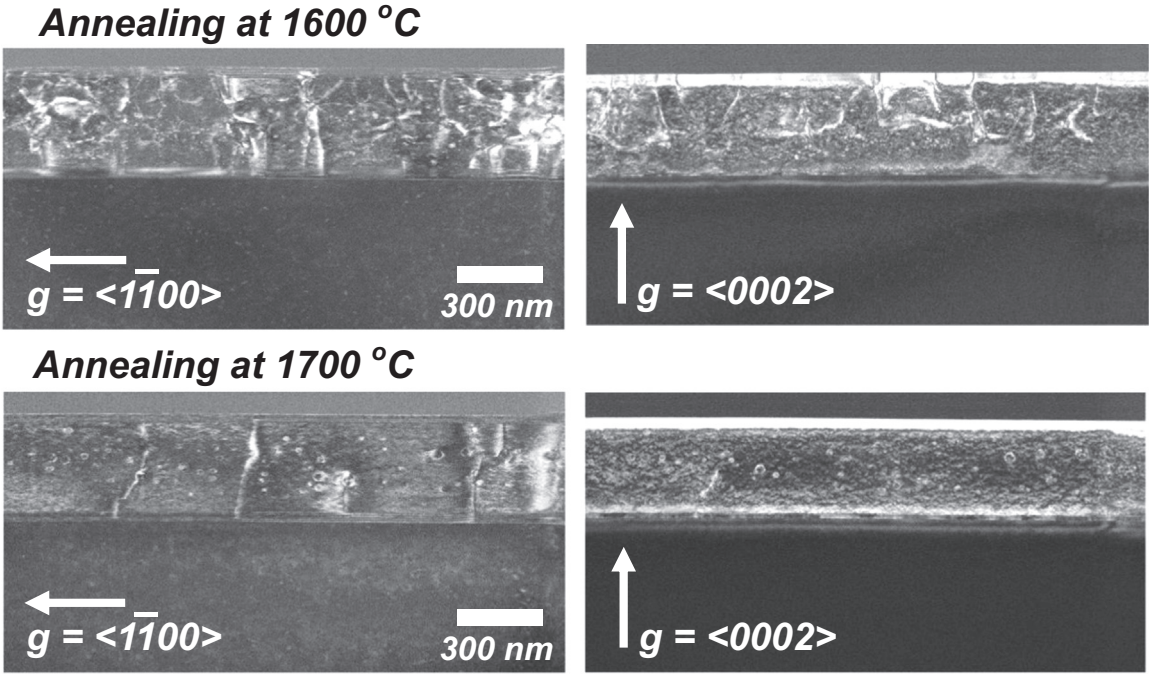

Fig. 8. Bright-field cross-sectional TEM images of 340-nm-thick sputtered AlN films after thermal annealing at 1600 and 1700 °C. The types of TDs are characterized under the two-beam condition with $g=<0002>$ and $g=<1\,\bar{1}00>$.

4. Conclusions

We have investigated the effects of thermal annealing in nitrogen ambient on sputtered AlN films grown on sapphire substrates. The surface morphology of the sputtered AlN films markedly changed from columnar-structure morphology to a step and terrace morphology after annealing at temperatures of 1600 °C and above. No pits were observed on the terrace owing to the successful suppression of thermal decomposition of the AlN film by overlapping AlN samples face-to-face. The FWHMs of the (0002)- ($10\bar{1}2$)-plane XRCs for the sputtered AlN films significantly decreased with increasing annealing temperature up to 1700 °C owing to the solid-phase reactions that occur at high annealing temperatures, which annihilated domain boundaries and concurrently increased the compressive stress in the films.

Acknowledgments

The authors gratefully acknowledge Mr. E. Komatsu and Mr. N. Terayama of Shinko Seiki Co., Ltd. for preparation and annealing of AlN films. This work was partially supported by the Akasaki Research Center of Nagoya University, Grants-in-Aid for Specially Promoted Research (No. 25000011) and Scientific Research (B) (No. 15H03556) from the Ministry of Education, Culture, Sports, Science and Technology (MEXT), and Strategic Foundational Technology Improvement Support Operation by Kansai Bureau of Economy, Trade and Industry.

References

[1] Y. Taniyasu, M. Kasu, T. Makimoto, Nature 441 (2006) 325.
[2] Y. Taniyasu, M. Kasu, N. Kobayashi, Appl. Phys. Lett. 81 (2002) 1255.
[3] Y. Shimahara, H. Miyake, K. Hiramatsu, F. Fukuyo, T. Okada, H. Takaoka, H. Yoshida, Appl. Phys. Express 4 (2011) 042103.
[4] R.T. Bondokov, S.G. Mueller, K.E. Morgan, G.A. Slack, S. Schujman, M.C. Wood, J. A. Smart, L.J. Schowalter, J. Cryst. Growth 310 (2008) 4020.
[5] C. Hartmann, J. Wollweber, A. Dittmar, K. Irmscher, A. Kwasniewski, F. Langhans, T. Neugut, M. Bickermann, Jpn. J. Appl. Phys. 52 (2013) 08JA06.
[6] S. –I. Nagahama, N. Iwasa, M. Senoh, T. Matsushita, Y. Sugimoto, H. Kiyoku, T. Kozaki, M. Sano, H. Matsumura, H. Umemoto, K. Chocho, T. Mukai, Jpn. J. Appl. Phys. 39 (2000) L647.
[7] J. Bai, M. Dudley, W.H. Sun, H.M. Wang, M.A. Khan, Appl. Phys. Lett. 88 (2006) 051903.
[8] S.Y. Karpov, Y.N. Makarov, Appl. Phys. Lett. 81 (2002) 4721.
[9] Y. Kida, T. Shibata, H. Naoi, H. Miyake, K. Hiramatsu, M. Tanaka, Phys. Status Solidi A 194 (2002) 498.
[10] H. Hirayama, S. Fujikawa, N. Noguchi, J. Norimatsu, T. Takano, K. Tsubaki, N. Kamata, Phys. Status Solidi A 206 (2009) 1176.
[11] H. Miyake, G. Nishio, S. Suzuki, K. Hiramatsu, H. Fukuyama, J. Kaur, N. Kuwano, Appl. Phys. Express 9 (2016) 025501.
[12] K. Hamanaka, T. Tachiki, T. Uchida, Jpn. J. Appl. Phys. 48 (2009) 125502.
[13] G. Ju, M. Highland, J.A. Eastman, R.J. Tissot, P. Zapol, P.M. Baldo, C. Thompson, P. H. Fuoss, Talk RR10.02 at Fall Material Research Society Meeting, Boston, 2015.
[14] F.A. Ponce, D. Cherns, W.T. Young, J.W. Steeds, Appl. Phys. Lett. 69 (1996) 770.